Energy-Dependent Multistability and Offset Boosting in a 5D Generalized Hamiltonian Conservative Hyperchaotic System

Ming Lyu(吕明)[1,2], Yihang Huang(黄艺航)[1], Wenbin Ji(姬文斌)[1], Zefeng Zhang(张泽峰)[1,2]

[1]Transportation Institute, Inner Mongolia University, Hohhot, 010070, China.

[2]Inner Mongolia Engineering Research Center for Intelligent Transportation Equipment, Hohhot, 010070, China.

August 30, 2026

Abstract

A new 5D generalized Hamiltonian conservative system with sine nonlinearity is proposed and investigated. Constructed from a constant antisymmetric structure matrix, the system preserves the generalized Hamiltonian framework while exhibiting enhanced nonlinear dynamics. The derived Hamiltonian function and the zero divergence property confirm that the system is energy conserving and volume preserving. Numerical analyses, including phase portraits, Poincaré sections, bifurcation diagrams, and Lyapunov exponent spectra, show that the system exhibits hyperchaotic behavior and a symmetric Lyapunov spectrum over a relatively wide parameter range. In addition, the system displays energy dependent multistability, coexistence of multiple conservative chaotic orbits under different initial conditions, and offset boosting dependent on initial values. These results enrich the class of high dimensional conservative hyperchaotic systems and provide a useful model for studying complex conservative dynamics within the generalized Hamiltonian framework.

Keywords: hyperchaos, multistability, offset boosting, generalized Hamiltonian

PACS: 05.45.-a, 05.45.Jn, 05.45.Pq

1. Introduction

Newtonian mechanics long dominated physical understanding, but 20th-century chaos theory overturned this by revealing deterministic systems can exhibit inherent randomness due to extreme sensitivity to initial conditions [1]. Chaos theory has become a major scientific revolution, applied in mathematics [2], physics [3], informatics [4], encryption [5,6], and communication security [7]. Nonlinear dynamics has deeply studied dissipative systems, but research on conservative systems, especially high-dimensional conservative chaos, is relatively weak. Conservative systems are a core theoretical foundation; their fractal structure provides an ideal model for order to disorder transitions and dynamical stability [8].

*Corresponding author: Zefeng Zhang E-mail: zhangzefeng_2021@163.com

Hamiltonian systems hold a significant position among conservative systems due to their physical background and geometric structure. However, classical Hamiltonian systems rely on standard symplectic structure [9], limiting their application to open systems with dissipation, external excitation, or non-conservative forces [10]. Generalized Hamiltonian system theory overcomes these limitations [11], offering inclusiveness to analyze energy exchange and stability within a unified geometric framework [12,13]. Hyperchaotic systems exhibit extreme complexity beyond chaos, elevating sensitivity to initial conditions and long-term unpredictability [14,15]. Conservative hyperchaotic systems share these advantages [16–18], generally possessing excellent statistical randomness suitable for image encryption [19]. Reference [20] presents a 5D Hamiltonian conservative hyperchaotic system via double/triple coupling of Euler equations. Reference [21] proposes an antisymmetric matrix construction with only constant terms and a multi-term state variable method with nonlinear terms. Reference [22] combines generalized Hamiltonian theory with a sine function to construct n-dimensional controllable multi-turbulent conservative chaotic systems. Reference [23] reveals hidden chaos and multistability coexistence in conservative chaotic systems. For an autonomous conservative chaotic system with a single random orbit, coordinate transformation, continuous function introduction, and parameter selection can generate infinite chaotic random orbits [24–27]. Different Hamiltonian energies may yield different multistability [28].

Motivated by the above, this study constructs and analyzes a high-dimensional nonlinear conservative system beyond traditional low-dimensional models. Based on the generalized Hamiltonian framework, a new 5D sine conservative system is developed using a constant antisymmetric structure matrix and sine nonlinearity. Its conservative nature is characterized via Hamiltonian function, equilibrium analysis, and zero divergence. Complex dynamical behaviors are systematically explored through theoretical analysis and numerical simulations, including hyperchaos, wide-parameter-range complexity, energy-dependent multistability, coexistence of conservative chaotic orbits, and initial-value-dependent offset boosting. The results enrich the study of high-dimensional conservative hyperchaotic systems and provide a useful model for further research on generalized Hamiltonian nonlinear dynamics and applications.

The remainder of this article is arranged as follows: Section 2 describes system construction using constant antisymmetric structure matrices. Section 3 analyzes dynamic behavior via numerical simulation. Section 4 reveals multistability and special dynamical laws. Section 5 discusses initial-value-based offset boosting. Section 6 evaluates pseudo-randomness via statistical test suites. Finally, the article is summarized.

2. A new type of 5D generalized Hamiltonian system

2.1. System construction

The differential equations of the generalized Hamiltonian system are as follows [19]:

$$\dot{\mathbf{x}} = \big(J(\mathbf{x}) - \varphi(\mathbf{x})\big)\nabla H(\mathbf{x}) + \boldsymbol{E} \tag{1}$$

After simplification, the energy dissipation term and input term were removed, resulting in the following equation:

$$\dot{\mathbf{x}} = J(\mathbf{x})\nabla H(\mathbf{x}) \tag{2}$$

Among them, $J(\mathbf{x})$ is called the structure matrix and is an antisymmetric matrix, which must satisfy

$J(\mathbf{x}) = -J^T(\mathbf{x})$, it describes how the energy is exchanged among the various state variables within the system and defines the interconnection structure of the system. $\nabla H(\mathbf{x})$ represents the gradient vector of the Hamiltonian function.

Most of the systems constructed in current literature are based on the 3D Euler equations. By adding all-zero rows and all-zero columns, higher-dimensional Euler equation subsystems are obtained. Then, through coupling, adding excitation and other methods, a generalized Hamiltonian system is obtained. The following modifications are introduced. The 3D Euler equation subsystem is extended to a 5D one, and make the structure matrix of it contain only constants without state variables, while ensuring that the constants in each row and each column are not all zero.

$$J_a(\mathbf{x}) = \begin{bmatrix} 0 & a & 0 & 0 & d \\ -a & 0 & b & 0 & 0 \\ 0 & -b & 0 & c & 0 \\ 0 & 0 & -c & 0 & 0 \\ -d & 0 & 0 & 0 & 0 \end{bmatrix} \tag{3}$$

To introduce sine nonlinearity, the third component of the Hamiltonian gradient is replaced by $sin(x_3)$. Substituting the resulting gradient and the antisymmetric structure matrix into Eq. (2) yields:

$$\dot{\mathbf{x}} = J_a(\mathbf{x})\nabla H(\mathbf{x}) \tag{4}$$

This leads to the new 5D sine conservative system as follows:

$$\begin{cases} \dot{x}_1 &= ax_2 + dx_5 \\ \dot{x}_2 &= -ax_1 + b\sin(x_3) \\ \dot{x}_3 &= -bx_2 + cx_4 \\ \dot{x}_4 &= -c\sin(x_3) \\ \dot{x}_5 &= -dx_1 \end{cases} \tag{5}$$

2.2. Energy analysis

Given that $\nabla H(\mathbf{x}) = (x_1, x_2, \sin(x_3), x_4, x_5)^T$, the Hamiltonian function can be deduced as:

$$H(\mathbf{x}) = \frac{1}{2}\left(x_1^2 + x_2^2 + x_4^2 + x_5^2\right) - \cos(x_3) \tag{6}$$

For systems that follow Hamiltonian dynamics, the rate of change of their total energy is the total derivative of the Hamiltonian function with respect to time:

$$\dot{H}(\mathbf{x}) = \nabla H^T(\mathbf{x})J(\mathbf{x})\nabla H(\mathbf{x}) \tag{7}$$

Substituting and performing the calculation yields a result of zero, which indicates that this system is Hamiltonian energy-conserving. Fig.1 further validates this result.

The Casimir function is an important concept in theoretical mechanics and Poisson geometry, and plays a crucial role in systems with a Poisson structure rather than the standard symplectic structure. According to the Lie-Poisson bracket definition, it is:

$$\dot{C} = \{C, H\} = \nabla C^T(\mathbf{x})J(\mathbf{x})\nabla H(\mathbf{x}) \tag{8}$$

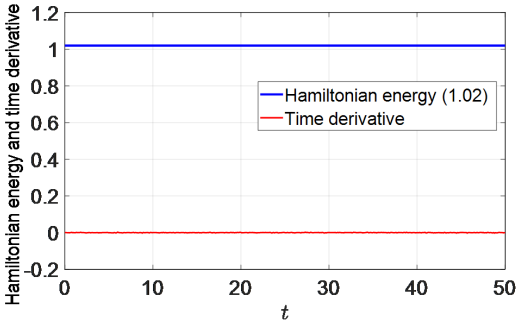


Fig. 1. Hamiltonian energy H defined in Eq. (6) for system (5) and its time derivative.

The Casimir function C is a function such that its Poisson bracket is zero with all other functions:

$$\{C, H\} = 0, \forall H \tag{9}$$

According to the definition, the expression of the Casimir function for this system can be obtained as follows:

$$C(\mathbf{x}) = x_2 + \frac{b}{c}x_4 - \frac{a}{d}x_5 \tag{10}$$

The corresponding formula for calculating Casimir power is:

$$\dot{C} = \nabla C^T(\mathbf{x})\dot{\mathbf{x}} \tag{11}$$

Substituting and calculating, the result is zero, which indicates that the system satisfies Casimir conservation.

2.3. Equilibrium point and dissipativity

The equilibrium points are obtained by setting the right-hand sides of system (5) to zero. After calculation, this system has infinitely many equilibrium points $(0,\ l,\ k\pi,\ \frac{b}{c}l,\ -\frac{a}{d}l)$. Here, l can take any value and k can take any integer.

Then, at the equilibrium point $(x_1^*, x_2^*, x_3^*, x_4^*, x_5^*)$, the system is linearized to obtain its Jacobian matrix $J_J(\mathbf{x}^*)$.

Set parameter $(a, b, c, d) = (6, 4, 6, 2)$, and let $|\lambda E - J_J(\mathbf{x}^*)| = 0$. The corresponding characteristic polynomial $P_i(\lambda)$ can be obtained.

Table 1 provides detailed data.

Table 1. Equilibrium points and their types.

Equilibrium point $(k \in \boldsymbol{Z},\ l \in \boldsymbol{R})$	Eigenvalue $\sigma,\ w,\ w_1,\ w_2 \in \boldsymbol{R}$	Type of equilibrium point
$(0,\ l,\ 2k\pi,\ \frac{b}{c}l,\ -\frac{a}{d}l)$	$(0,\ \pm jw,\ \pm jw_1)$	Center type
$(0,\ l,\ (2k+1)\pi,\ \frac{b}{c}l,\ -\frac{a}{d}l)$	$(0,\ \pm\sigma,\ \pm jw_2)$	Saddle type

The computational method for the system's dissipativity is as follows:

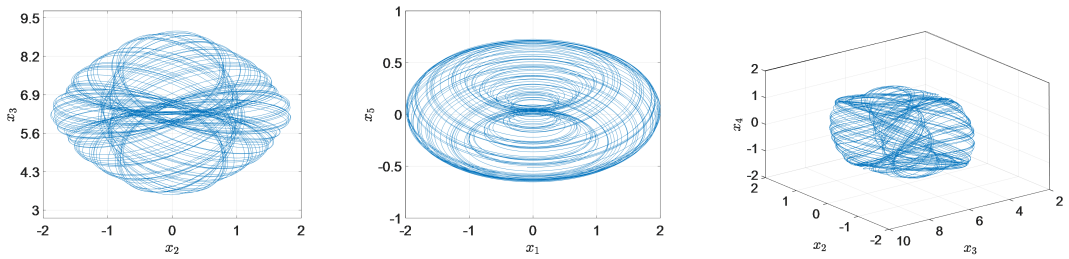
$$\nabla f = \frac{\partial \dot{x}_1}{\partial x_1} + \frac{\partial \dot{x}_2}{\partial x_2} + \frac{\partial \dot{x}_3}{\partial x_3} + \frac{\partial \dot{x}_4}{\partial x_4} + \frac{\partial \dot{x}_5}{\partial x_5} = 0 \tag{12}$$

The zero divergence indicates phase volume preservation. Together with the conservation of the Hamiltonian function, this confirms the conservative nature of system (5). Its complex dynamical behaviors are further investigated numerically in Section 3.

3. System dynamics analysis

3.1. Phase diagrams

The phase portraits provide an intuitive visualization of the dynamical behaviors of system (5). The system is Hamiltonian energy conserving and phase-volume preserving, as demonstrated in Section 2. For the initial condition $(x_1, x_2, x_3, x_4, x_5) = (0.1, 0.1, \pi, 0.1, 0.1)$ and parameters $a = 6, b = 4, c = 6$, and $d = 2$, Figs.2(a) and 2(b) show the trajectories projected onto the x_2-x_3 and x_1-x_5 planes, respectively. Fig.2(c) further presents the trajectory in the x_2-x_3-x_4 space, illustrating the complex phase-space structure of the system.



(a) (b) (c)

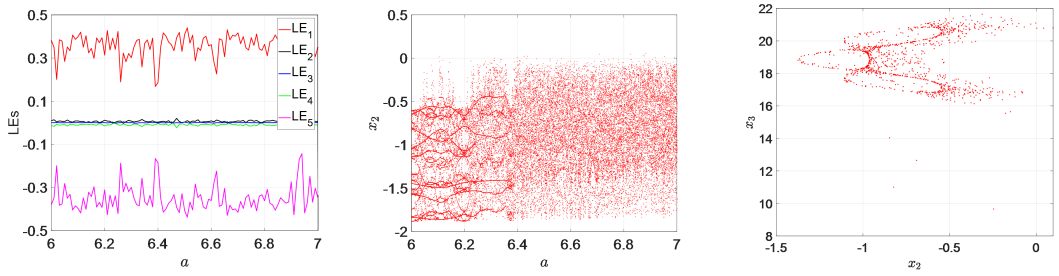
Fig. 2. Phase diagrams: (a) Phase diagram in the x_2-x_3 plane, (b) Phase diagram in the x_1-x_5 plane, (c) Phase diagram in the x_2-x_3-x_4 space.

3.2. Lyapunov exponent spectrum and bifurcation diagram

This work calculates its parameter-a-related Lyapunov exponent spectrum. As a core metric, the spectrum characterizes average exponential divergence or convergence rate of phase-space trajectories, and its sign distribution determines system dynamic types. For $a \in [6, 7]$, with $b = 4, c = 6$, and $d = 2$, Fig.3(a) shows that the system possesses two positive Lyapunov exponents, LE_1 and LE_2, confirming its hyperchaotic behavior. The zero exponent LE_3 corresponds to tangential direction of the autonomous flow, while LE_4 and LE_5 are negative. In addition, the Lyapunov spectrum exhibits an approximately symmetric distribution. The sum of all Lyapunov exponents is approximately zero within numerical precision, which is consistent with the volume-preserving property of the system. The corresponding bifurcation diagram is displayed in Fig.3(b).

3.3. Poincaré section

For geometric dynamic description, the Poincaré section on hyperplane $x_1 = 0$ is plotted with given parameters. Fig.3(c) depicts the projection of x_2 and x_3 on this section. Distinct from discrete points of periodic motion and smooth closed curves of quasi-periodic motion for regular systems, this section presents dense, diffuse and non completely disordered scattered point clouds filling a finite region with inherent internal structure, which is the typical feature of phase space chaotic motion. It demonstrates non repetitive and stochastic system trajectories attached to complex geometric structures, and long-term trajectory evolution outlines the overall point cloud boundary. This geometric result matches Lyapunov exponent spectrum analysis.

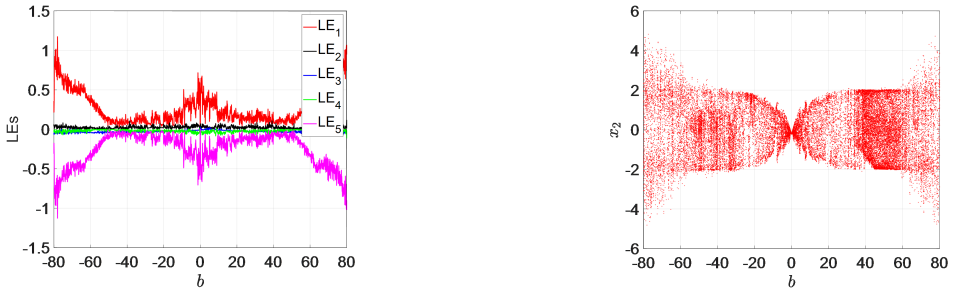


(a) (b) (c)

Fig. 3. Combined analysis: (a) Lyapunov exponent spectrum varying with parameter a, (b) Bifurcation diagram varying with parameter a, (c) Poincaré section in the x_2-x_3 plane.

3.4. Wide parameter range

The system possesses numerically stable chaotic behavior in a wide parameter range, which sustains stable chaotic states and avoids dynamic performance degradation. With fixed parameters $(a, c, d) = (6, 6, 2)$ and variable parameter $b \in [-80, 80]$, Fig.4(a) plots the system Lyapunov exponent spectrum. The third Lyapunov exponent fluctuates near zero, and the rest four exponent curves are axisymmetric about the horizontal axis. As shown in Fig.4(b), except for the degenerate case $b = 0$, the system exhibits chaotic dynamics over a broad parameter range.



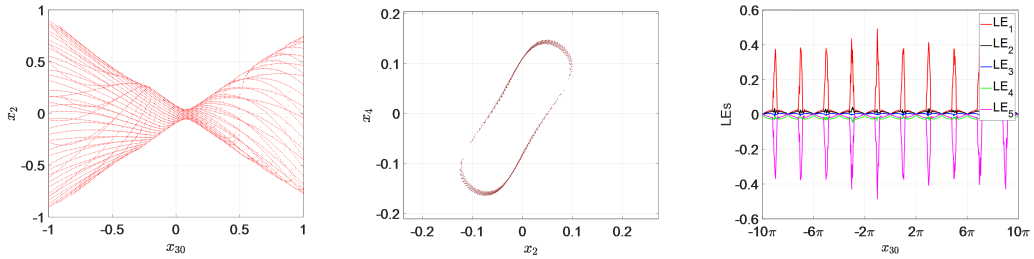
(a) (b)

Fig. 4. Combined analysis: (a) Lyapunov exponent spectrum varying with parameter b, (b) Bifurcation diagram varying with parameter b.

4. Other dynamic behaviors of the system and multistability analysis

4.1. Analysis of other dynamic behaviors

System (5) has infinite equilibrium points categorized into center and saddle types. This equilibrium distribution usually predicts chaotic attractors in dissipative systems, whereas conservative systems own fundamentally different dynamics. Thus, System (5) can exhibit complex conservative chaotic orbits. Set parameters $(a, b, c, d) = (6, 4, 6, 2)$, and the bifurcation diagram varying with initial value x_{30} is displayed in Fig.5(a). A narrow band emerges at $x_{30} \approx 0.12$, suggesting quasi-periodic state, which is validated by the closed discrete curve in Poincaré section (Fig.5(b)). Given trigonometric function characteristics, the x_{30} range is expanded to $[-10\pi, 10\pi]$. Its Lyapunov exponent spectrum in Fig.5(c) shows that, owing to the periodicity of the sine nonlinearity, the dynamical regimes repeat with a period of 2π as the initial value x_{30} varies, following the sequence of quasi-periodic motion, weak chaos, strong chaos, weak chaos, and quasi-periodic motion.



(a) (b) (c)

Fig. 5. Combined analysis: (a) Bifurcation diagram varying with initial value x_{30}, (b) Poincaré section in the x_2-x_4 plane, (c) Lyapunov exponent spectrum varying with initial value x_{30}.

Fig.6(a) and 6(b) plot Hamiltonian energy spatial distributions on initial x_1-x_5 and x_2-x_3 planes, with color bars denoting Hamiltonian energy values. The Hamiltonian energy rises with increased system initial values. Low initial values correspond to low energy levels with quasi-periodic and weak chaotic motions, which transform into chaotic states as energy increases.



(a) (b)

Fig. 6. Combined energy diagrams: (a) 3D surface diagram of Hamiltonian energy varying with x_{10}-x_{50}, (b) 3D surface diagram of Hamiltonian energy varying with x_{20}-x_{30}.

4.2. Multistability related to energy

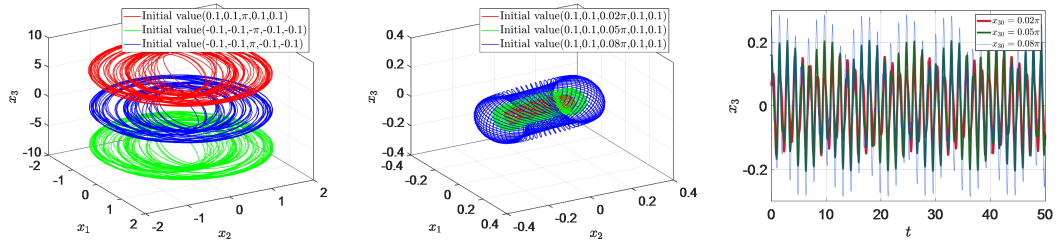
4.2.1. Coexisting orbits under the same energy level

Different initial values produce diverse trajectories under equal energy. To verify this conclusion, three initial values (0.1, 0.1, π, 0.1, 0.1), (-0.1, -0.1, -π, -0.1, -0.1), (-0.1, -0.1, π, -0.1, -0.1) are selected. Fig.7(a) presents coexisting chaotic trajectories under diverse initial conditions, which evolve independently in fixed phase-space regions without mutual interference and enrich system dynamic behaviors. Besides, these chaotic trajectories share similar shapes, which is attributed to the inherent energy conservation and invariant phase volume of conservative Hamiltonian systems.

4.2.2. Coexisting orbits under different energy levels

Further research shows the system features unequal-energy coexisting orbits for distinct initial conditions. Set system parameters $(a, b, c, d) = (6, 4, 6, 2)$, three initial values $x_{30} = 0.02\pi, 0.05\pi, 0.08\pi$ are adopted with other initial values fixed. The x_1-x_2-x_3 phase diagram is displayed in Fig.7(b). Different initial values generate coexisting orbits with disparate sizes; higher Hamiltonian energy is associated with a larger spatial extent of the orbit and stronger chaotic behavior. The matching time series in Fig.7(c) shows rising oscillation amplitude with increased x_{30}, which enhances system chaoticity and randomness. The consistent expansion of time series and phase space orbits suggests that increasing energy can enhance the chaotic activity within the investigated

range. This result matches Lyapunov exponent analysis, verifying energy is a key factor regulating the system chaotic level.



(a) (b) (c)

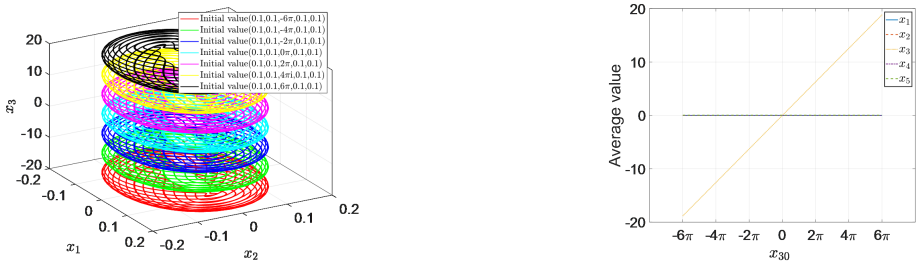
Fig. 7. Phase diagrams and time series diagram of the system: (a) Phase diagram in the x_1-x_2-x_3 space, (b) Phase diagram in the x_1-x_2-x_3 space, (c) Time series diagram.

5. Offset boosting control

Offset boosting is a current research hotspot, which provides a concise and efficient control strategy to regulate system phase-space position and dynamic behaviors. Existing offset boosting strategies are divided into controller-dependent type and initial value-dependent type. Previous analysis obtains system equilibrium points $(0,\ l,\ k\pi,\ \frac{b}{c}l,\ -\frac{a}{d}l)$, where l is an arbitrary constant and k is an arbitrary integer. Adjusting initial parameters l_0 and k_0 changes system initial values and equilibrium points, further shifting the position of conservative flow. Consequently, the studied system presents typical initial offset boosting characteristic.

5.1. Perfectly homogeneous offset in quasi-periodic state

The offset boosting behavior is verified by tuning k_0 with fixed parameters $a = 6,\ b = 4,\ c = 6,\ d = 2$. As aforementioned, the system evolves from $x_3 = 0$ with periodic state transition among quasi-periodicity, weak chaos and strong chaos. For even $|k|$, k_0 varies from -6 to 6 with an interval of 2. Fig.8(a) depicts the x_1-x_2-x_3 phase diagrams with changing k_0. All phase diagrams share identical global and local structures despite disparate spatial positions, proving complete homogeneous phase-diagram shift of the system. Fig.8(b) displays the average values of state variables, which can judge trajectory offset: monotonic curves represent obvious offset behavior, while irregular curves fail to confirm dynamic shift. Only the average value of x_3 presents a monotonic increasing straight line, and other variables keep zero average values. It reveals that the conservative flow shifts along the positive x_3-axis with the variation of initial value x_{30}.

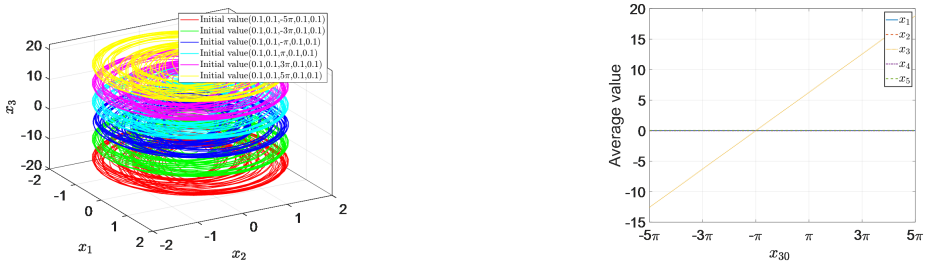


(a) (b)

Fig. 8. Combined analysis: (a) Phase diagram in the x_1-x_2-x_3 space, (b) Average value diagram.

5.2. Offset in Chaotic State

With the same fixed parameters $a = 6,\ b = 4,\ c = 6,\ d = 2$, k_0 ranges from -5 to 5 with a step of 2 for odd $|k|$. Fig.9(a) presents the corresponding x_1-x_2-x_3 phase diagrams under varied k_0. All phase trajectories have consistent global and local structures but different spatial positions, confirming homogeneous phase trajectory offset of the system. The average value diagram in Fig.9(b) demonstrates that only x_3 average value increases monotonically, and other variables maintain zero average values. Similarly, the conservative flow shifts along the positive x_3-axis with the increase of initial x_{30}.



(a) (b)

Fig. 9. Combined analysis: (a) Phase diagram in the x_1-x_2-x_3 space, (b) Average value diagram.

5.3. Other offset boosting control

Previous discussions only investigate x_3-based initial value-dependent offset boosting. Nevertheless, the equilibrium point reveals that l_0 is also an arbitrary constant to realize extra offset boosting control strategies. With fixed parameters $a = 6,\ b = 4,\ c = 6,\ d = 2$, guided by the equilibrium family, four pairs of l_0 and k_0 are selected as $(l_0\ , k_0\ ) = (-0.2, -3), (-0.1, -1), (0.1, 1), (0.2, 3)$. The corresponding initial conditions are chosen as $(0.1,\ l_0,\ k_0\pi,\ \frac{b}{c}l_0,\ -\frac{a}{d}l_0)$. Fig.10(a) plots the x_1-x_2-x_3 phase diagrams with varied l_0 and k_0. Four conservative hyperchaotic orbits share similar shapes and shift along positive x_3-axis, with orbital intervals determined by l_0 and k_0. The corresponding time series in Fig.10(b) show that increasing l_0 and k_0 triggers overall upward offset of x_3 waveform, accompanied by polarity transition from single polarity to dual polarity and back to single polarity.



(a) (b)

Fig. 10. Combined analysis: (a) Phase diagram in the x_1-x_2-x_3 space, (b) Time series diagram.

6. Statistical Randomness Test

The NIST SP 800-22 test suite with 15 sub-tests is adopted to assess randomness of chaotic sequences from System (5). Sequence randomness is judged by P-value with significance level $\alpha = 0.01$, and qualified pass rates are mandatory. Test results in Table 2 show the minimum P-value of 0.021999 from NonOverlappingTemplate test exceeds 0.01, and all pass rates satisfy standard thresholds. The system-generated sequences exhibit favorable statistical randomness, indicating the potential applicability of the chaotic sequences generated by the proposed system to image encryption, similar to existing hyperchaos-based encryption studies [29–31].

Table 2. NIST test results.

system (5)			
Sequence	Test items	P value	Pass rate
1	Frequency	0.816537	0.99
2	BlockFrequency	0.867692	0.99
3	CumulativeSums	0.834308	1
4	Runs	0.779188	0.98
5	LongestRun	0.401199	0.96
6	Rank	0.678686	1
7	FFT	0.964295	0.99
8	NonOverlappingTemplate	0.021999	0.96
9	OverlappingTemplate	0.924076	1
10	Universal	0.719747	0.99
11	ApproximateEntropy	0.191687	0.99
12	RandomExcursions	0.862344	1
13	RandomExcursionsVariant	0.931952	1
14	Serial	0.455937	0.99
15	LinearComplexity	0.554420	0.99

7. Conclusion

In this paper, a new 5D generalized Hamiltonian conservative hyperchaotic system with sine nonlinearity is constructed based on a constant antisymmetric structure matrix. Theoretical derivation of the Hamiltonian function and zero-divergence calculation verify its energy-conserving and phase-volume-preserving properties. The dynamical behaviors of the system are numerically investigated using phase portraits, Lyapunov exponent spectra, bifurcation diagrams, and Poincaré sections. The system maintains hyperchaos over a wide parameter range and exhibits several characteristic conservative phenomena, including energy-dependent multistability, coexistence of conservative chaotic orbits, and initial-value-dependent offset boosting. The NIST SP 800-22 tests further demonstrate the favorable statistical randomness of the generated chaotic sequences, indicating their potential for applications in image encryption and information security. This work enriches the family of high-dimensional conservative hyperchaotic systems and provides a useful model for generalized Hamiltonian nonlinear dynamics research. Despite these results, the present study is mainly limited to theoretical analysis and numerical simulation. Hardware implementation and experimental verification have not yet been carried out, and the practical performance of the proposed system in specific encryption applications remains to be systematically evaluated. Future work will therefore focus on hardware realization, such as FPGA implementation, and the development of chaotic encryption schemes based on the proposed system. In addition, the

present construction strategy may be extended to higher-dimensional conservative chaotic systems.

Acknowledgments

This work is supported by the Natural Science Foundation of Inner Mongolia Autonomous Region of China (No. 2025QN01013; No. 2025MS01007), the Inner Mongolia University Young Academic Talent Research Initiation Project (No. 10000-A24299053), the 2024 Research Support Project for Introducing Talents at the Autonomous Region Level of Inner Mongolia Autonomous Region (No. 22200-252906), and National Natural Science Foundation of China (No. 12302016).

References

[1] Wang C P, Wang X Y, Zhang C and Xia Z Q 2017 Geometric correction based color image watermarking using fuzzy least squares support vector machine and bessel k form distribution *Signal Processing* **134** 197

[2] Talatahari S and Azizi M 2020 Optimization of constrained mathematical and engineering design problems using chaos game optimization *Computers & Industrial Engineering* **145** 106560

[3] Zhou N R, Hu L L, Huang Z W, Wang M M and Luo G S 2024 Novel multiple color images encryption and decryption scheme based on a bit-level extension algorithm *Expert Systems with Applications* **238** 122052

[4] Wang B, Zou F C and Cheng J 2018 A memristor-based chaotic system and its application in image encryption *Optik* **154** 538

[5] Wang X Y and Liu L T 2013 Cryptanalysis of a parallel sub-image encryption method with high-dimensional chaos *Nonlinear Dynamics* **73** 795

[6] Mou J, Cai C, Gao S, Zhou N R and Zhang Y S 2025 A Second-Order Memristor-Based Rulkov Neuron: Design, Dynamical Analysis and Application in Hierarchical Decryption of 3D Model *IEEE Internet of Things Journal* **12** 43470

[7] An X L, Liu S Y, Xiong L, Zhang J G and Li X Y 2024 Mixed gray-color images encryption algorithm based on a memristor chaotic system and 2D compression sensing *Expert Systems with Applications* **243** 122899

[8] Cang S J, Wu A G, Zhang R Y, Wang Z H and Chen Z Q 2018 Conservative chaos in a class of nonconservative systems: Theoretical analysis and numerical demonstrations *International Journal of Bifurcation and Chaos* **28** 1850087

[9] Cang S J, Li Y, Kang Z J and Wang Z H 2020 A generic method for constructing n-fold covers of 3D conservative chaotic systems *Chaos: An Interdisciplinary Journal of Nonlinear Science* **30** 033103

[10] Ma Y J, Mou J, Banerjee S and Miao M 2023 A quartic nonlinear flux-controlled memristor model and its application in chaotic system *Applied and Computational Mathematics* **22** 317

[11] Ji'e M S, Duan S K and Wang L D 2023 Another n-D Conservative Chaotic/Hyperchaotic System *IEEE Transactions on Circuits and Systems II: Express Briefs* **71** 1451

[12] Ji'e M S, Yan D W, Wang L D and Duan S K 2021 Hidden attractor and multistability in a novel memristor-based system without symmetry *International Journal of Bifurcation and Chaos* **31** 2150168

[13] Jia H Y, Li W, Wang H J, Han X G and Wang S M 2024 FPGA Implementation for a Class of Generalized Hamiltonian Conservative Chaotic Systems Based on Integrated 4D Euler Equations with Multistability *International Journal of Bifurcation and Chaos* **34** 2450188

[14] Dong E Z, Zhang Z J, Yuan M F, Ji Y H, Zhou X S and Wang Z H 2019 Ultimate boundary estimation and topological horseshoe analysis on a parallel 4D hyperchaotic system with any number of attractors and its multi-scroll *Nonlinear Dynamics* **95** 3219

[15] Dong E Z, Yuan M F, Du S Z and Chen Z Q 2019 A new class of Hamiltonian conservative chaotic systems with multistability and design of pseudo-random number generator *Applied Mathematical Modelling* **73** 40

[16] Li Y X, Wang M F, Chang H, Wang H and Chen G R 2024 A hyperchaotic memristive system with extreme multistability and conservativeness *Nonlinear Dynamics* **112** 3851

[17] Yu F, Tan B H, He T, He S Q, Huang Y Y, Cai S and Lin H R 2025 A wide-range adjustable conservative memristive hyperchaotic system with transient quasi-periodic characteristics and encryption application *Mathematics* **13** 726

[18] An X L, Li Z F, Xue R, Xiong L and Zhang L 2025 Construction of Multi-Scroll Conservative Chaotic System and Its Application in Image Encryption *Journal of Electronics & Information Technology* **47** 4470

[19] Liu X L, Tong X J, Wang Z and Zhang M 2022 Construction of controlled multi-scroll conservative chaotic system and its application in color image encryption *Nonlinear Dynamics* **110** 1897.

[20] Zhang Z F, Huang L L, Liu J, Guo Q, Du X L and Yu C D 2023 Modeling method of a class of 5D Hamiltonian conservative hyperchaotic systems with adjustable signal amplitude *Physica Scripta* **98** 105224

[21] Leng X X, Zhang C K and Du B X 2022 Modeling methods and characteristic analysis of new Hamiltonian and non-Hamiltonian conservative chaotic systems *AEU-International Journal of Electronics and Communications* **152** 154242

[22] Dong E Z, Li R H and Du S Z 2021 A multi-directional controllable multi-scroll conservative chaos generator: Modelling, analysis, and FPGA implementation *Chinese Physics B* **30** 020505

[23] Jia H Y, Chen Z G, Shi W X and Qi G Y 2022 A new generalized Hamiltonian chaotic system with transient quasi-periodic flows and intermittent chaos *International Journal of Bifurcation and Chaos* **32** 2250022

[24] Zhang Z F, Huang L L, Xiang J H and Liu S 2021 Dynamic study of a new five-dimensional conservative hyperchaotic system with wide parameter range *Acta Physica Sinica* **70** 230501

[25] Zhang Z F and Huang L L 2022 A new 5D Hamiltonian conservative hyperchaotic system with four center type equilibrium points, wide range and coexisting hyperchaotic orbits *Nonlinear Dynamics* **108** 637

[26] Jiao X D, Wang X Y, Yuan M F, Tao J, Sun H, Sun Q L and Chen Z Q 2024 Dynamics modeling of a memristor-based Rucklidge chaotic system: Multistability, offset boosting control and FPGA implementation *Chinese Journal of Physics* **90** 823

[27] Jiao X D, Yuan M F, Tao J, Sun H, Sun Q L and Chen Z Q 2023 Memristor hyperchaos in a generalized Kolmogorov-type system with extreme multistability *Chinese Physics B* **32** 010507

[28] Li R H, Dong E Z, Tong J G and Du S Z 2022 A new autonomous memristive megastable oscillator and its Hamiltonian-energy-dependent megastability *Chaos: An Interdisciplinary Journal of Nonlinear Science* **32** 013127

[29] Hong Y, Duan X Y, Su J M, Wang Z P and Fang S H 2025 A novel approach to visual image encryption: 2D hyperchaos, variable Josephus, and 3D diffusion *Chinese Physics B* **34** 040504

[30] Han Z T, Cao Y H, Banerjee S and Mou J 2025 Hybrid image encryption scheme based on hyperchaotic map with spherical attractors *Chinese Physics B* **34** 030503

[31] Tian J X, Jin S C, Zhang X Q, Yang S W and Shi D X 2024 Remote sensing image encryption algorithm based on novel hyperchaos and an elliptic curve cryptosystem *Chinese Physics B* **33** 050502